INTERNAL MEDICINE

CASE REPORT

Parkinsonism in Type I Gaucher's Disease

Kaori Itokawa[1], Naotoshi Tamura[1], Nobutaka Kawai[2], Kunio Shimazu[1] and Kenji Ishii[3]

Abstract

The majority of patients with type I Gaucher's disease never develop neurological signs or symptoms. However, several case reports of Parkinson's disease associated with type I Gaucher's disease have been published, suggesting a genetic link between the two diseases. Hence, detailed clinical investigations are required when the two diseases occur simultaneously, in order to determine whether this is coincidental or whether a true association is present. We present a Japanese man in whom parkinsonism was associated with type I Gaucher's disease. Findings of brain positron tomography (PET) and metaiodobenzylguanidine (MIBG) cardiac scintigraphy are presented.

Key words: Gaucher's disease, parkinsonism, metaiodobenzylguanidine myocardial SPECT, fluorodeoxyglucose PET, levodopa

(DOI: 10.2169/internalmedicine.45.1790)

Case Report

A 42-year-old man with type I Gaucher's disease was admitted to our hospital with an 8-month history of poor mobility of the right leg. His intelligence seemed normal; he was working in computer engineering with no reported difficulties. Gaucher's disease had been diagnosed at the age of 31, based on the following typical findings; hepatosplenomegaly, Gaucher cells on bone marrow biopsy, reduction in β-glucosidase activity, and L444P/R463C mutation of the glucocerebrosidase gene on genetic analysis. Enzyme replacement therapy had been started at the age of 34, and signs of Gaucher's disease, including anemia and hepatosplenomegaly, were absent at the present admission. On neurological examination, cogwheel-type rigidity was evident in the right upper and lower limbs, and poor arm swing was noted on walking, but tremor was absent. Mental function was normal. However, his speech was limited and monotonous, and facial expression was masked. Finger tapping was slow on the right side but retropulsion was absent. Deep tendon reflexes were normal and pathological reflexes were absent. Dysdiadochokinesis was absent. Brain MRI failed to demonstrate any lesions. PET using [F-18] fluorodeoxyglucose (FDG) as a tracer showed hypometabolism in the frontal and parietal cortices, although metabolism in the striatum was well preserved (Fig. 1). [I-123] MIBG myocardial SPECT revealed persistent low uptake in the inferoposterior area on early phase and complete absence of MIBG uptake in this area on delayed phase. [Tc-99m] tetrofosmin SPECT revealed low uptake in the septum and inferior areas (Fig. 2), suggesting that the reduced MIBG uptake in these areas was due to old myocardial infarction. However, ECG was normal, and the patient denied any history of apparent myocardial infarction. Levodopa-carbidopa therapy was commenced at an initial dose of 100 mg daily and subsequently increased to 200 mg daily, following which his gait disturbance and hand immobility were resolved.

Discussion

In their case report of Parkinson's disease associated with type I Gaucher's disease, Tayebi et al (1) described a crossover between the glucocerebrocidase gene (GBA) and metaxin gene. The metaxin gene is involved in mitochondrial function, which may be altered in Parkinson's disease. Aharon-Peretz et al (2) reported that 31.3% of cases with Parkinson's disease exhibit genetic susceptibility. These studies suggest a common genetic basis for both Gaucher's disease and Parkinson's disease. To date, no anomaly in the

[1] Department of Neurology, Saitama Medical University, Saitama, [2] Department of Hematology, Saitama Medical University, Saitama and [3] Positron Medical Center, Tokyo Metropolitan Institute of Gerontology, Tokyo

Received for publication February 21, 2006; Accepted for publication June 20, 2006

Correspondence to Dr. Kaori Itokawa, Department of Neurology, Saitama Medical School, 38 Moro Hongo, Moroyama-cho, Iruma-gun, Saitama 350-0495

DOI: 10.2169/internalmedicine.45.1790

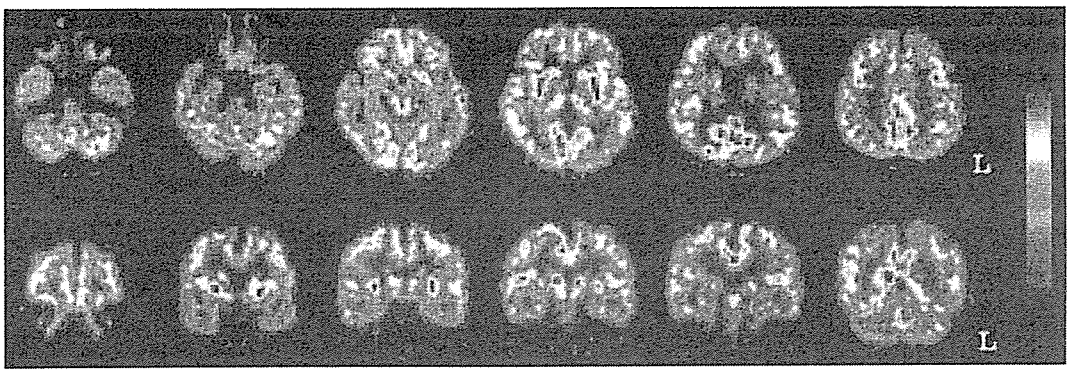

Figure 1. [F-18] FDG PET shows hypometabolism in the frontal and parietal cortices, but metabolism in the striatum is well preserved.

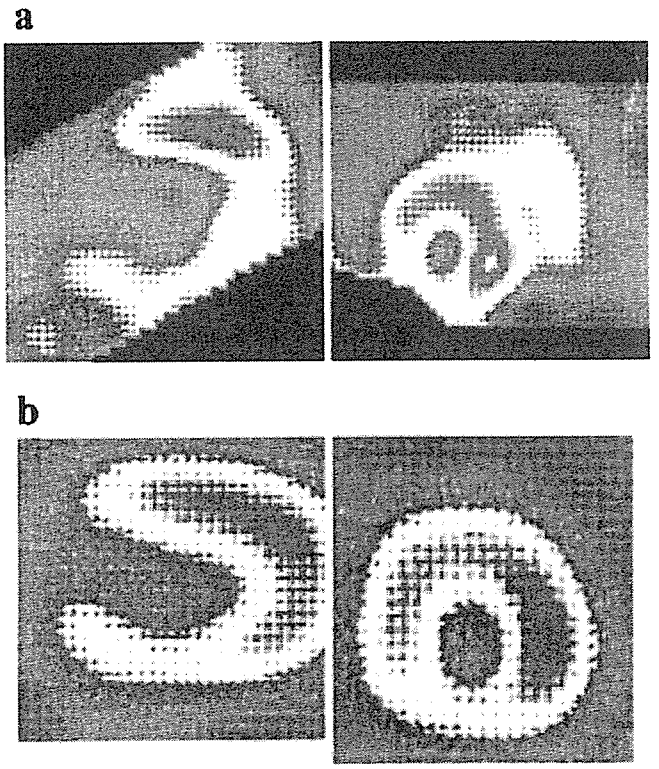

Figure 2. MIBG myocardial SPECT shows persistent low uptake in the infero-posterior area (a); however, [Tc-99m] tetrofosmin SPECT also reveals low uptake inthe sptum and inferior areas (b), suggesting that reduced MIBG uptake is due to cardiac infarction rather than sympathetic denervation. H/M ratio is 1.84.

GBA/metaxin gene has been identified in any form of hereditary parkinsonism, but we do not consider the coexistence of Gaucher's disease and Parkinson's disease to be a mere chance association.

However, the clinical features of Parkinson's disease in type I Gaucher's disease differ somewhat from those of typical Parkinson's disease (1-7). In most published cases, the age at onset of parkinsonism was younger than that seen in typical Parkinson's disease, resting tremor was not evident, and the effect of levodopa was relatively poor. However, further clinical investigations were not described in these articles. In the present case, parkinsonism responded well to levodopa therapy, and [F-18] fluorodeoxyglucose (FDG) PET revealed that function of the striatum, a postsynaptic structure of the nigro-striatal dopaminergic pathway, was well preserved. These findings are identical to those of idiopathic Parkinson's disease.

However, onset as early as the 5th decade of life, absence of resting tremor, and relative preservation of myocardial MIBG uptake are not typical features of idiopathic Parkinson's disease. In particular, MIBG myocardial scintigraphy has been established as a useful tool to distinguish idiopathic Parkinson's disease from other parkinsonian syndromes such as multiple system atrophy and progressive supranuclear palsy. Myocardial uptake of MIBG is completely absent, indicating cardiac sympathetic denervation, in the majority of cases of idiopathic Parkinson's disease, even in the earlier stages, while it is well-preserved in other parkinsonian syndromes (8-11). In the present case, apart from a partial defect of MIBG uptake probably due to old myocardial infarction, MIBG scintigraphy did not indicate a reduced uptake. Normal uptake of MIBG in the present case may represent a lack of Levy body pathology, since MIBG uptake is also preserved in autosomal recessive juvenile parkinsonism with PARK2 anomaly (10).

It is noteworthy that the clinical features of parkinsonism in Gaucher's disease differ distinctly from those of typical Parkinson's disease. While we do not consider the coexistence of Gaucher's disease and Parkinson's disease to represent a mere chance association, it is noteworthy that the clinical features of such cases differ distinctly from those of typical Parkinson's disease. Gaucher's disease-related parkinsonism may account for a small number of cases of Parkinson's disease.

DOI: 10.2169/internalmedicine.45.1790

References

1. Tayebi N, Callahan M, Madike V, et al. Gaucher disease and parkinsonism: a phenotypic and genotypic characterization. Mol Genet Metab **73**: 313-321, 2001.
2. Aharon-Peretz J, Rosenbaum H, Gershoni-Baruch R. Mutations in the glucocerebrosidase gene and Parkinson's disease in Ashkenazi Jews. N Engl J Med **351**: 1972-1977, 2004.
3. Neudorfer O, Giladi N, Elstein D, et al. Occurrence of Parkinson's syndrome in type I Gaucher disease. Q J M **89**: 691-694, 1996.
4. Varkonyi J, Simon Z, Soos K, Poros A. Gaucher disease type I complicated with Parkinson's syndrome. Haematologia **32**: 271-275, 2002.
5. Macaczka M, Rucinska M, Skotnicki AB, Jurczal W. Parkinson's syndrome preceding clinical manifestation of Gaucher's disease. Am J Hematol **61**: 216-217, 1999.
6. McKeran RO, Bradbury P, Taylor D, Stern G. Neurological involvement in type I (adult) Gaucher's disease. J Neurol Neurosurg Psychiatry **48**: 172-175, 1985.
7. Neil JF, Glew RH, Peters SP. Familial psychosis and diverse neurologic abnormalities in adult-onset Gaucher's disease. Arch Neurol **36**: 95-99, 1979.
8. Yoshita M. Differentiation of idiopathic Parkinson's disease from striatonigral degeneration and progressive supranuclear palsy using iodine-123 metaiodobenzylguanidine myocardial scintigraphy. J Neurol Sci **155**: 60-67, 1998.
9. Orimo S, Ozawa E, Nakade S, Sugimoto T, Mizusawa H. ^{123}I-metaiodobenzylguanidine myocardial scintigraphy. J Neurol Neurosurg Psychiatry **67**: 189-194, 1999.
10. Orimo S, Amino T, Yokochi M, et al. Preserved cardiac sympathetic nerve accounts for normal cardiac uptake of MIBG in PARK2. Mov Disord **20**: 1350-1353, 2005.
11. Druschky A, Hilz MJ, Platsch G, et al. Differentiation of Parkinson's disease and multiple system atrophy in early disease by means of I-123-MIBG-SPECT. J Neurol Sci **175**: 3-12, 2000.

Cerebral networks for spontaneous and synchronized singing and speaking

Yoko Saito[a,b,c], Kenji Ishii[b], Kazuo Yagi[c], Itaru F. Tatsumi[d] and Hidehiro Mizusawa[a]

[a]Department of Neurology and Neurological Science, Tokyo Medical and Dental University, [b]Positron Medical Center, Tokyo Metropolitan Institute of Gerontology, [c]Department of Radiological Science, Tokyo Metropolitan University of Health Sciences and [d]Language, Cognition and Brain Science Research Group, Tokyo Metropolitan Institute of Gerontology, Tokyo, Japan

Correspondence and requests for reprints to Kenji Ishii, MD, Positron Medical Center, Tokyo Metropolitan Institute of Gerontology, 1-1 Nakacho, Itabashi-ku, Tokyo 173-0022, Japan
Tel: +81 3 3964 3241 ext. 3503; fax: +81 3 3964 2188; e-mail: ishii@pet.tmig.or.jp

Received 8 September 2006; accepted 26 September 2006

Singing in unison is usually easier than singing alone, but the neural mechanism underlying these two contrasting modes of singing remains unknown. We investigated neural correlates of singing by a functional magnetic resonance imaging study focusing on the capacities of spontaneity and synchronization and compared them with those of speaking. The left inferior frontal gyrus appears important for self-generation of text in singing and speaking without auditory input, whereas the left posterior planum temporale plays a key role in synchronizing both text and melody, in combination with the bilateral inferior parietal lobule for singing along, and with the left angular gyrus for speaking in chorus. These findings indicate that text and melody are not processed symmetrically or parallel in singing a well-learned song. *NeuroReport* 17:1893–1897 © 2006 Lippincott Williams & Wilkins.

Keywords: functional magnetic resonance imaging, inferior frontal gyrus, planum temporale, singing, speaking, spontaneity, synchronization

Introduction

When singing, we occasionally sing alone; often, however, we sing along with others. This singing may or may not be accompanied by instrumental music. Similarly, although we usually speak alone, we occasionally speak together in a group, for example, during group chanting. Neural networks for singing should involve control mechanisms of two contrasting modes: self-production and synchronized production. It is essential for the self-production of a song to retrieve and represent the internally stored lyrics, rhythm, and melody without the help of external sensory information. On the other hand, it is important for the synchronized production of a song to monitor the external auditory information and to concurrently render synchronous control of articulation. In terms of simple voluntary movements such as finger tapping, there have been several reports that have focused on the differences in the central mechanisms for self-paced movements and externally cued movements [1]. Recently, investigations have been conducted on more complex tasks of finger tapping to external auditory rhythms, such as synchronization compared with syncopation [2], and finger tapping following various rhythms [3]. This work aroused an interest in auditory–motor correlations rather than the spontaneous control of voluntary movements. No previous studies have been found focusing on the capacities of spontaneity and synchronization for singing. It may be useful to investigate the neural mechanism underlying singing from the standpoint of spontaneity and synchronization for the planning of therapy for apraxia of speech, aphasia, and dementia [4]. The purpose of this study was to investigate the neural mechanisms underlying the two different modes of singing: singing alone and singing along. In this paper, we use the term 'spontaneous' singing to refer to the self-production of a well-learned song without the help of external sensory information, and it does not imply any improvisational behavior.

Some recent works have investigated the neural networks from the viewpoint of simple pitch and melody generation [5,6]. Most of the previous studies that investigated singing, however, showed contrasting mechanisms for language and music [7,8]. These studies have shown a symmetric view of language and music: the inferior frontal gyrus, anterior insula, and superior temporal gyrus in the right hemisphere play a predominant role in singing, whereas the homologous regions in the left hemisphere are mainly involved in speaking. On the basis of a conventional model of cerebral lateralization, some lesion studies have indicated that language and music are dealt with parallel networks [9,10]. On the other hand, behavioral experiments and recent neuroimaging studies have suggested that processes for language and music are not completely separate [11–15]. The complete viewpoint of the inter-relationship between text and melody processing in singing remains unknown. To elucidate the neural correlates underlying spontaneous and synchronized processes in singing, we contrasted them with those in speaking in order to address the issue of integration and segregation of music and language in singing.

Materials and methods

Participants

We studied 20 normal right-handed Japanese nonmusicians (19–24 years old; 10 men and 10 women) without any neurological or hearing impairment, after obtaining their

written informed consent. None had experienced any specific training for singing or playing an instrument, except for ordinary schoolwork. Most of them regularly listened to music, but sang only occasionally in day-to-day life. This study was approved by the Ethics Committee of the Tokyo Metropolitan University of Health Sciences.

Experimental paradigm and stimuli

The task design consisted of the following conditions: (i) overtly singing 'Umi' (The Sea) – a very popular song among the Japanese – alone (Sg_solo); (ii) overtly singing Umi in synchronization with the auditory presentation of the song, including the melody and lyrics (Sg_syn); (iii) listening to the singing undertaken in the previous task (L_Sg); (iv) overtly reciting alone the lyrics of Umi without the melody (Sp_solo); (v) overtly reciting Umi along with an auditory presentation of the lyrics (Sp_syn); (vi) listening to the reciting undertaken in the previous task (L_Sp); and (vii) rest condition. The processes involved in each task are summarized in Table 1. For the participants, it was easy to not only sing the song, but also recite the lyrics because the lyrics had a seven-and-five syllable meter, a characteristic style observed in traditional Japanese poems. The auditory stimuli (sampling rate, 44.1 kHz) of singing and speaking were recorded by a female singer, without adding any effect. The averaged rate, fundamental frequency (F0), and intensity of the auditory stimuli were recorded (mean $\pm$ SD) to be 1.60 ± 0.14 moras/s, 221 ± 43 Hz, and 69.9 ± 8.1 dB SPL (SPL: sound pressure level), respectively, for singing, and 2.5 ± 0.13 moras/s, 215 ± 43 Hz, and 69.9 ± 6.5 dB SPL, respectively, for speaking. The rate of presentation alone was significantly different between singing and speaking ($P < 0.01$, paired t-test). In the sound-proof room, the participants underwent prescan training. During training, they practiced singing synchronously with an auditory presentation (Sg_syn task), and this was done until they sang the entire song correctly by themselves without making any mistakes in the lyrics, melody, rhythm and tempo, as assessed by the examiner. Prescan training for the speaking version was also done in the same way.

Data acquisition

Magnetic resonance imaging (MRI) data acquisition was performed with a 1.5-T scanner (Signa; General Electric, Milwaukee, Wisconsin) by using a gradient-echo echoplanar imaging-sequence (TR, 5000 ms; TE, 35.1 ms; flip angle, 60°; matrix size, 128×128; field of view, 24×24 cm^2; and 21 slices with 5 mm thickness). The functional MRI procedure involved six runs that were labeled Sg_solo, Sg_syn, L_Sg, Sp_solo, Sp_syn, and L_Sp and the order was counterbalanced across the participants. One run consisted of six blocks in which the rest block (60 s) alternated with the task block (60 s), and the six runs were performed at 5-min intervals. The participants gently bit disposable wooden bite-bars with their molars during scanning to minimize head and jaw motion artifacts associated with articulation, but the articulation was intelligible. During the scan, the performance of the participant was monitored for text and melody components by experimenters. After each scan, we asked the participants whether they could hear the auditory input and their own song/speech clearly during the scan and if they could perform the task as instructed.

Data analysis

Analysis of the functional MRI data was performed using SPM99 (Wellcome Department of Cognitive Neurology, University College London, London, UK) implemented on MATLAB (Mathworks, Natick, Massachusetts, USA). After

Table 1 Components involved in each task

Components		Articulation; self-monitoring		External perception		Spontaneous production		Synchronized production	
Task		Text	Melody	Text	Melody	Text	Melody	Text	Melody
Spontaneous singing: Sg_solo		○	○	-	-	○	○	-	-
Synchronized singing: Sg_syn		○	○	○	○	-	-	○	○
Listening to the song: L_Sg		-	-	○	○	-	-	-	-
Spontaneous speaking: Sp_solo		○	-	-	-	○	-	-	-
Synchronized speaking: Sp_syn		○	-	○	-	-	-	○	-
Listening to the speech: L_Sp		-	-	○	-	-	-	-	-
Paired t-test									
A_1	Sg_solo > Sg_syn								
A_2	Sg_syn > Sg_solo								
B_1	Sp_solo > Sp_syn								
B_2	Sp_syn > Sp_solo								
C_1	Sg_solo > Sp_solo								
C_2	Sg_syn > Sp_syn								
D_1	Sp_solo > Sg_solo								
D_2	Sp_syn > Sg_syn								

Circles indicate that the task includes the component, whereas dashes indicate the task that does not include the component. Light gray boxes show components related to spontaneous processes, and black boxes show components related to synchronized processes.
Sg_solo, spontaneous singing; Sg_syn, synchronized singing; Sp_solo, spontaneous speaking; Sp_syn, synchronized speaking.

realignment, normalization, and smoothing (full-width at half-maximum, 6 mm), the activated voxels were identified using the general linear model approach [16]. In each participant, a single summary 'contrast' image of a given condition was produced by convolving the images with a standard hemodynamic response function. Next, one-sample *t*-test based on the random effects model was applied contrasting passive listening conditions compared with rest: (L_Sg – rest) and (L_Sp – rest). Then, paired *t*-test was applied contrasting one task condition with another task condition, to determine the brain regions that were specifically activated by each component of the task: (Sg_solo – rest) vs. (Sg_syn – rest), (Sp_solo – rest) vs. (Sp_syn – rest), (Sg_solo – rest) vs. (Sp_solo – rest), and (Sg_syn – rest) vs. (Sp_syn – rest) (Table 1). The specific activations of each paired *t*-test was inclusively masked with the minuend contrast to avoid the detection of pseudo activation caused by deactivation (decrease in signal intensity relative to the rest condition) in the subtrahend contrast [17]. For instance, contrast of (Sg_solo – rest) > (Sg_syn – rest) were inclusively masked by (Sg_solo – rest). The threshold for the pass criterion of the inclusive mask was set to $P<0.001$ (uncorrected). For all statistical comparisons, we used a height threshold of $P<0.05$ (corrected) at the cluster statistics level and a spatial extent of $K=30$ voxels. Montreal Neurologic Institute coordinates were converted to the original coordinate system of Talairach and Tounoux (1988) by Matthew Brett's transformations.

Results

At the postscan interview, all participants reported that they could hear their own song/speech and the auditory input of singing/speaking clearly during the scan. In the passive listening tasks, the L_Sg activated the bilateral Heschl's gyrus, bilateral upper bank of the superior temporal sulcus, bilateral posterior part of the planum temporale, left planum polare, right dorsal premotor cortex, and right supplementary motor area, whereas the L_Sp activated the bilateral Heschl's gyrus, bilateral superior temporal sulcus, left posterior planum temporale, and right planum polare.

Specific activations for spontaneous processes and for synchronized processes in singing and speaking are summarized in Table 2a and displayed in Fig. 1. Specific activations for singing processes and for speaking processes in spontaneous and synchronized conditions are summarized in Table 2b. No significant activated area that was involved in speaking but not in singing (D_1 and D_2) existed.

Discussion

The spontaneous tasks selectively activated the left inferior frontal gyrus in contrast to the synchronized tasks: the left anterolateral part of the inferior frontal gyrus in singing and the left pars triangularis of the inferior frontal gyrus in speaking. On the basis of our task design, it can be interpreted that the activation in the left pars triangularis of the inferior frontal gyrus in speaking is specific to the spontaneous generation of text, but it is also possible that

Table 2a Activations for spontaneity and synchronization in each singing and speaking

Brain regions		Singing (Fig. 1a)				Speaking (Fig. 1b)			
		x	*y*	*z*	*Z*-value	*x*	*y*	*z*	*Z*-value
Spontaneous process (green)			Sg_solo > Sg_syn				Sp_solo > Sp_syn		
Anterolateral part of the IFG	L	−32	37	−5	4.72				
Pars triangularis of the IFG	L					−42	25	1	4.61
Synchronized process (red)			Sg_syn > Sg_solo				Sp_syn > Sp_solo		
Posterior planum temporale	L	−44	−36	12	5.12	−48	−33	2	5.26
	R	40	−33	10	4.58				
Anterior edge of the IPL	L	−54	−27	21	4.73				
	R	50	−20	24	4.68				
Angular gyrus	L					−56	−49	25	4.93

Sg_solo, spontaneous singing; Sg_syn, synchronized singing; Sp_solo, spontaneous speaking; Sp_syn, synchronized speaking; IFG, inferior frontal gyrus; IPL, inferior parietal lobule.

Table 2b Activations for singing and speaking in each spontaneity and synchronization

Brain regions		Spontaneous process				Synchronized process			
		x	*y*	*z*	*Z*-value	*x*	*y*	*z*	*Z*-value
Singing process			Sg_solo > Sp_solo				Sg_syn > Sp_syn		
Dorsal premotor cortex	R	50	12	36	4.79	50	2	40	5.01
IFG/Anterior insula	R	45	29	−5	4.62	40	23	−5	4.64
Anterior cingulate cortex	R	2	23	36	4.02	2	17	34	4.55
Planum temporale	R	52	−22	6	5.16	60	−29	11	4.97
Planum polare	R					48	−4	10	4.42
Middle insula	R					46	2	−3	4.83
Anterior edge of the IPL	L					−50	−22	26	4.34
Speaking process			Sp_solo > Sg_solo				Sp_syn > Sg_syn		
			NS				NS		

Talairach coordinates and the *Z*-values of peak activation; activated regions detected by paired *t*-test: $P<0.05$ corrected for multiple comparisons, using an inclusive mask: $P<0.001$, uncorrected.
Sg_solo, spontaneous singing; Sg_syn, synchronized singing; Sp_solo, spontaneous speaking; Sp_syn, synchronized speaking; IFG, inferior frontal gyrus; IPL, inferior parietal lobule; L, left; R, right.

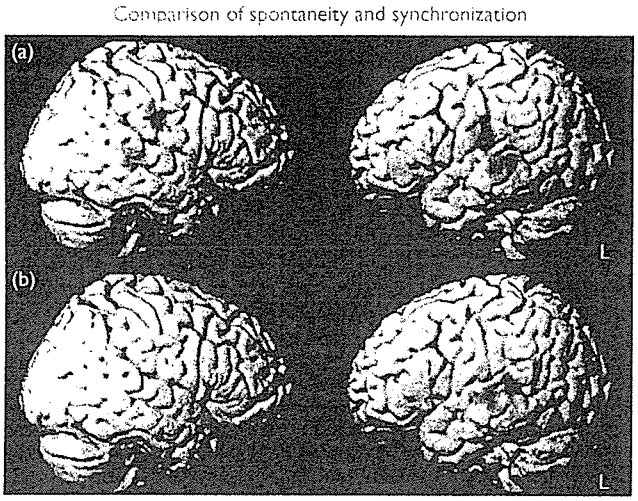

Fig. 1 Activations specific to the spontaneous process (green) and those specific to the synchronized process (red). (a) Singing; (b) speaking ($P < 0.05$, corrected).

the activation of the left anterolateral part of inferior frontal gyrus in singing is related not only to the spontaneous generation of text but also to that of melody [13]. Strong evidence indicates thats the major role played by the left inferior frontal gyrus is language generation in various aspects such as phonology, semantics, and syntax [18]. Damage to the left inferior frontal gyrus could cause a condition called dynamic aphasia, in which the patient faces a difficulty in producing spontaneous speech without any difficulty in naming, repetition, and comprehension. Robinson *et al.* [19] attributed this condition to the inability to select an appropriate verbal response from a large number of competing candidates. Warren *et al.* [20] reported the case of a patient suffering from dynamic aphasia owing to left inferior frontal gyrus atrophy who was able to generate melody without lyrics. Therefore, activity in the left inferior frontal gyrus may be related to the spontaneous generation of text rather than melody. Text generation in singing, however, is more complex than that in speaking, considering the need for supplying words for the tune and rhythm. This may explain the difference in the location of the left inferior frontal gyrus activation in singing and speaking. Another possible interpretation of the activation of left inferior frontal gyrus is associated with the increasing motor preparation [15] or cognitive control in spontaneous tasks.

On the other hand, activations specific for the spontaneous generation of melody, which imply the actions complementing the left inferior frontal gyrus activation, were not observed. The right inferior frontal gyrus and right anterior insula have been reported to be involved in melody generation [8,13]. In our study, these areas were found to be active specifically for singing but not for speaking under both spontaneous and synchronized conditions. These results suggest that the roles of the right inferior frontal gyrus and right anterior insula are not exclusive for the spontaneous condition. In addition, the right dorsal premotor cortex was observed as a singing-specific area regardless of spontaneous, synchronized, or listening conditions, implying that the right dorsal premotor cortex is involved in preparing the motor components of music production, such as melody and rhythm [6]. These findings suggest that melody and text generation in spontaneous singing of a well-learned song are not treated in parallel; melody might subsequently be generated along with text generation. To investigate the specific regions involved in the spontaneous generation of melody, the spontaneity and synchronization of pure melody, avoiding the influence of text, need to be examined in the future.

As the synchronized tasks relative to the spontaneous tasks contain two major components of external perception and synchronized production, activations to be detected by paired *t*-tests need to be interpreted in the light of the activation by passive listening tasks. Among the activations observed that are specific to the synchronized tasks, the posterior planum temporale was also activated by listening tasks. The left posterior planum temporale has been reported as common areas between covert singing and speaking and passive listening to songs and speech [14]. Moreover, the left posterior planum temporale has been reported to be involved in the processing and primary storage of various complex sound patterns [21]. Considering these points, the role of the left posterior planum temporale is not a passive perceptional function; it appears to play a more active role of bridging the external auditory information with further judgment and motor planning. The cortical region surrounding the left posterior Sylvian fissure in the posterior parietal–temporal boundary has been reported to be implicated in verbal working memory [22], auditory–motor integration for speech [23], and auditory–motor integration for both speech and music [24]. Our results suggest that the left posterior planum temporale plays an essential role in the synchronized processing of both melody and text, in combination with more specific regions: in combination with the bilateral anterior edge of the inferior parietal lobule and right posterior planum temporale, for synchronized singing, and with the left angular gyrus, for synchronized speaking. Activations in the left anterior edge of the inferior parietal lobule, right posterior planum temporale, right planum polare, and right middle insula were detected in synchronized singing as compared with synchronized speaking, suggesting that these areas are essential for processing melody rather than text under synchronized conditions [24,25].

Conclusion

Our results elucidate the neural networks of spontaneous and synchronized singing. The left inferior frontal gyrus may be essential for the spontaneous generation of text: the anterolateral part of the left inferior frontal gyrus in singing and pars triangularis of the left inferior frontal gyrus in speaking. In contrast, the right inferior frontal gyrus and right anterior insula are involved in melody generation regardless of spontaneous or synchronized conditions. On the other hand, the left posterior planum temporale plays the role of an auditory hub for synchronization of text and melody, in combination with the bilateral anterior edge of the inferior parietal lobule in singing and the left angular gyrus in speaking. Our findings suggest that text and melody in a well-learned song are not dealt with by symmetric or parallel networks. The neural mechanisms of spontaneous and synchronized singing will provide us with the basics to understand the neural mechanisms for a higher level of spontaneity (e.g. propositional speech and improvisation music), other forms of music (e.g. instrumental

melody and percussion), and their further application in education and rehabilitation.

Acknowledgement

We would like to thank Takashi Kodama, MSc, for the technical support.

References

1. Rao SM, Harrington DL, Haaland KY, Bobholz JA, Cox RW, Binder JR. Distributed neural systems underlying the timing of movements. *J Neurosci* 1997; 17:5528–5535.
2. Jantzen KJ, Steinberg FL, Kelso JA. Brain networks underlying human timing behavior are influenced by prior context. *Proc Natl Acad Sci U S A* 2004; 101:6815–6820.
3. Chen JL, Zatorre RJ, Penhune VB. Interactions between auditory and dorsal premotor cortex during synchronization to musical rhythms. *Neuroimage* 2006; 32:1771–1781.
4. Gotell E, Brown S, Ekman SL. Influence of caregiver singing and background music on posture, movement, and sensory awareness in dementia care. *Int Psychogeriatr* 2003; 15:411–430.
5. Perry DW, Zatorre RJ, Petrides M, Alivisatos B, Meyer E, Evans AC. Localization of cerebral activity during simple singing. *Neuroreport* 1999; 10:3453–3458.
6. Langheim FJ, Callicott JH, Mattay VS, Duyn JH, Weinberger DR. Cortical systems associated with covert music rehearsal. *Neuroimage* 2002; 16:901–908.
7. Riecker A, Ackermann H, Wildgruber D, Dogil G, Grodd W. Opposite hemispheric lateralization effects during speaking and singing at motor cortex, insula and cerebellum. *Neuroreport* 2000; 11:1997–2000.
8. Jeffries KJ, Fritz JB, Braun AR. Words in melody: an $H_2{}^{15}O$ PET study of brain activation during singing and speaking. *Neuroreport* 2003; 14: 749–754.
9. Peretz I, Kolinsky R, Tramo M, Labrecque R, Hublet C, Demeurisse G, Belleville S. Functional dissociations following bilateral lesions of auditory cortex. *Brain* 1994; 117:1283–1301.
10. Hebert S, Racette A, Gagnon L, Peretz I. Revisiting the dissociation between singing and speaking in expressive aphasia. *Brain* 2003; 126:1838–1850.
11. Serafine ML, Crowder RG, Repp BH. Integration of melody and text in memory for songs. *Cognition* 1984; 16:285–303.
12. Koelsch S, Gunter TC, v Cramon DY, Zysset S, Lohmann G, Friederici AD. Bach speaks: a cortical 'language-network' serves the processing of music. *Neuroimage* 2002; 17:956–966.
13. Brown S, Martinez MJ, Parsons LM. Music and language side by side in the brain: a PET study of the generation of melodies and sentences. *Eur J Neurosci* 2006; 23:2791–2803.
14. Callan DE, Tsytsarev V, Hanakawa T, Callan AM, Katsuhara M, Fukuyama H, Turner R. Song and speech: brain regions involved with perception and covert production. *Neuroimage* 2006; 31:1327–1342.
15. Ozdemir E, Norton A, Schlaug G. Shared and distinct neural correlates of singing and speaking. *Neuroimage* 2006; 33:628–635.
16. Friston KJ, Holmes AP, Worsley KJ, Poline JB, Frith CD, Frackowiak RS. Statistical parametric mapping in functional imaging: a general linear approach. *Human Brain Mapp* 1995; 2:189–210.
17. Makuuchi M, Kaminaga T, Sugishita M. Brain activation during ideomotor praxis: imitation and movements executed by verbal command. *J Neurol Neurosurg Psychiatry* 2005; 76:25–33.
18. Vigneau M, Beaucousin V, Herve PY, Duffau H, Crivello F, Houde O, *et al.* Meta-analyzing left hemisphere language areas: phonology, semantics, and sentence processing. *Neuroimage* 2006; 30:1414–1432.
19. Robinson G, Blair J, Cipolotti L. Dynamic aphasia: an inability to select between competing verbal responses? *Brain* 1998; 121:77–89.
20. Warren JD, Warren JE, Fox NC, Warrington EK. Nothing to say, something to sing: primary progressive dynamic aphasia. *Neurocase* 2003; 9:140–155.
21. Griffiths TD, Warren JD. The planum temporale as a computational hub. *Trends Neurosci* 2002; 25:348–353.
22. Jonides J, Schumacher EH, Smith EE, Koeppe RA, Awh E, Reuter-Lorenz PA, *et al.* The role of parietal cortex in verbal working memory. *J Neurosci* 1998; 18:5026–5034.
23. Wise RJ, Scott SK, Blank SC, Mummery CJ, Murphy K, Warburton EA. Separate neural subsystems within 'Wernicke's area'. *Brain* 2001; 124: 83–95.
24. Hickok G, Buchsbaum B, Humphries C, Muftuler T. Auditory-motor interaction revealed by fMRI: speech, music, and working memory in area Spt. *J Cogn Neurosci* 2003; 15:673–682.
25. Brown S, Martinez MJ, Hodges DA, Fox PT, Parsons LM. The song system of the human brain. *Cogn Brain Res* 2004; 20:363–375.

Annals of Nuclear Medicine Vol. 20, No. 8, 569–573, 2006

A feasibility study of [^{11}C]SA4503-PET for evaluating sigma$_1$ receptor occupancy by neuroleptics: the binding of haloperidol to sigma$_1$ and dopamine D_2-like receptors

Kiichi ISHIWATA,* Kenji ODA,** Muneyuki SAKATA,*** Yuichi KIMURA,* Kazunori KAWAMURA,* Keiichi ODA,* Toru SASAKI,* Mika NAGANAWA,*,**** Kunihiro CHIHARA,*** Yoshiro OKUBO***** and Kenji ISHII*

*Positron Medical Center, Tokyo Metropolitan Institute of Gerontology
**Section of Liaison Psychiatry and Palliative Medicine, Graduate School of Tokyo Medical and Dental University
***Graduate School of Information Science, Nara Institute of Science and Technology
****JSPS Research Fellow, Tokyo
*****Department of Psychiatry, Nippon Medical School

We investigated feasibility of positron emission tomography (PET) with [^{11}C]SA4503 for evaluating the sigma$_1$ receptor occupancy rate by neuroleptics. Haloperidol, which is well known to bind dopamine D_2-like receptor (D2R) as well as to be a representative non-selective antagonist for sigma$_1$ receptor (σ1R), was selected as a model drug. Three healthy male subjects underwent 60-min [^{11}C]raclopride-PET and 90-min [^{11}C]SA4503-PET scans successively at a 120-min interval twice in a day for baseline measurement and on another day for haloperidol-loading measurement 16 hours after peroral administration of 3 mg of haloperidol. Binding potential (BP) of [^{11}C]raclopride and [^{11}C]SA4503 was quantitatively evaluated and the σ1R and D2R occupancy rates were determined. D2R occupancy rates by haloperidol were 64% and 62% in the caudate and putamen, respectively, 16 h after the administration, while σ1R occupancy rates were approximately 80% in all seven regions investigated including the caudate, putamen and cerebellum 18 h after the administration, suggesting that the σ1R receptor occupancy rate by haloperidol was slightly larger than the D2R receptor occupancy rate. We concluded that [^{11}C]SA4503-PET can be used for evaluating the σ1R occupancy rates by neuroleptics or other drugs.

Key words: [^{11}C]SA4503, sigma$_1$ receptor, receptor occupancy, haloperidol, positron emission tomography

INTRODUCTION

In vivo evaluation of receptor occupancy by antipsychotic and antihistamineric drugs in the human brain has been investigated extensively by positron emission tomography (PET) and single-photon emission computed tomography (SPECT) with appropriate radioligands.[1,2] These *in vivo* techniques are very useful for evaluating the therapeutic effects of the drugs, for determining appropriate dosages and for developing new drugs. So far, the occupancy of drugs for dopamine, serotonin and histamine receptors were mainly evaluated.[1–3] It is also well known that a number of neuroleptics possess moderate to high affinity for sigma binding sites, suggesting the possibility that sigma receptors mediate some of the antipsychotic effects of neuroleptics.[4,5] The physiological and pathophysiological roles of the sigma receptors remain under investigation and are considered as targets of pharmaceuticals for several diseases.[6] However, the sigma receptor occupancy rates by the therapeutic drugs have not been evaluated in humans by PET or SPECT, because no *in vivo* selective radioligand was available. Recently,

Received May 18, 2006, revision accepted July 21, 2006.
For reprint contact: Kiichi Ishiwata, Ph.D., Positron Medical Center, Tokyo Metropolitan Institute of Gerontology, 1–1 Nakacho, Itabashi-ku, Tokyo 173–0022, JAPAN.
E-mail: ishiwata@pet.tmig.or.jp

Table 1 Binding potential (BP) of [^{11}C]SA4503 and [^{11}C]raclopride in the baseline and haloperidol-loading conditions and receptor occupancy rates by haloperidol

	[^{11}C]SA4503			[^{11}C]Raclopride		
	Binding potential*		Sigma$_1$ receptor occupancy	Binding potential*		Dopamine D_2 receptor occupancy
	Baseline	Haloperidol	%	Baseline	Haloperidol	%
Caudate	16.0 ± 1.4	3.0 ± 0.5	81.2 ± 4.9	3.3 ± 0.5	1.2 ± 0.3	64.4 ± 8.9
Putamen	18.5 ± 3.2	3.2 ± 0.5	81.9 ± 6.2	3.9 ± 0.6	1.5 ± 0.3	62.3 ± 7.8
Cerebellum	29.0 ± 1.9	5.7 ± 0.7	80.4 ± 3.1			
Frontal lobe	20.8 ± 0.8	3.8 ± 0.8	81.5 ± 3.9			
Temporal lobe	26.1 ± 4.1	4.7 ± 1.2	81.4 ± 7.0			
Occipital lobe	20.3 ± 2.1	3.9 ± 1.3	81.1 ± 4.7			
Thalamus	20.9 ± 2.1	4.8 ± 0.7	76.9 ± 2.7			

Data show mean ± SD (n = 3). *Binding potential was evaluated based on a 2-tissue 3-compartment model for [^{11}C]SA4503[9] and a reference tissue model for [^{11}C]raclopride.[15]

we have developed [^{11}C]SA4503 as a selective PET ligand for sigma$_1$ receptor (σ1R),[7–9] and clinically applied it to measuring σ1Rs of patients with Alzheimer's and Parkinson's disease.[6,10]

Previously, we investigated in mice using a tissue dissection technique whether [^{11}C]SA4503 is available as an *in vivo* probe for evaluating the σ1R occupancy rates by neuroleptics using PET.[11] We selected haloperidol and two other dopamine D_2-like receptor (D2R) ligands which had high affinity for D2Rs and different affinity for sigma receptors. In the present study, we measured the σ1R occupancy rate by haloperidol in the human brain by [^{11}C]SA4503-PET as a feasibility study that [^{11}C]SA4503-PET can be applied to evaluating σ1R occupancy rates by therapeutics. We also performed [^{11}C]raclopride-PET in the same subjects for evaluating D2R occupancy rates by haloperidol.

MATERIALS AND METHODS

The study protocol was approved by the Institutional Ethical Committee. Three male volunteers (24 ± 4 years old) who were healthy according to the history and clinical investigations and showed no abnormality on brain MRI participated in the present study, with written informed consent obtained from each. All subjects underwent two PET scans with [^{11}C]raclopride and [^{11}C]SA4503 twice on two separate days: first for baseline measurement and 2–6 weeks later for haloperidol-loading conditions. On each day [^{11}C]raclopride-PET was started late morning and two hours later [^{11}C]SA4503-PET was followed, because [^{11}C]raclopride shows a faster clearance rate from the brain than [^{11}C]SA4503. On the second day the subjects were perorally given 3 mg of haloperidol 16 hours before [^{11}C]raclopride-PET.

The PET camera used was SET-2400W (Shimadzu, Kyoto, Japan), which has an axial field-of-view of 20 cm and acquires 63 slices at a center-to-center interval of 3.125 mm.[12] The injected doses of [^{11}C]raclopride[13] were 336 ± 17 MBq/5.6 ± 2.9 nmol (specific activity 74 ± 36 TBq/mmol) and those of [^{11}C]SA4503[7] were 512 ± 160 MBq/13.6 ± 9.3 nmol (specific activity 51 ± 26 TBq/mmol). After transmission scanning with a rotating [^{68}Ge]/[^{68}Ga] line source to correct for attenuation, [^{11}C]raclopride was intravenously injected into the subject, and then a 60-min PET scanning in 2D mode (10 sec × 6 frames, 30 sec × 3 frames, 60 sec × 5 frames, 150 sec × 5 frames, and 300 sec × 8 frames) was performed without arterial blood sampling. In the second PET scan with [^{11}C]SA4503, a 90-min dynamic scan in 2D mode (10 sec × 6 frames, 30 sec × 3 frames, 60 sec × 5 frames, 150 sec × 5 frames, and 300 sec × 14 frames) was carried out together with arterial blood sampling at 10, 20, 30, 40, 50, 60, 70, 80, 90, 100, 110, 120, 135 and 150 sec and 3, 5, 7.5, 10, 15, 20, 30, 40, 50, 60, 70, 80 and 90 min. The radioactivity levels in plasma were measured for radioactivity for gamma-counter and the time-activity curve (TAC) of plasma was calculated as Bq/m*l* and SUV. Metabolites of [^{11}C]SA4503 in the plasma sampled at 3, 10, 20, 30, 40 and 60 min were analyzed by high-performance liquid chromatography as previously described.[7]

The tomographic images were reconstructed using a Fourier rebinning algorithm[14] and a filtered backprojection method with Butterworth filter (cutoff frequency 1.25 cycle/cm and order 2). The data were collected in a 128 × 128 × 63 matrix, and the voxel size was 2 × 2 × 3.125 mm. Voxel counts were calibrated to activity concentration (Bq/m*l*). Regions of interest (ROIs) were placed over the caudate, putamen, cerebellum, frontal lobe, temporal lobe, occipital lobe and thalamus and on the PET images with reference to MRI. TACs of these ROIs were calculated as Bq/m*l* and SUV. For quantitative measurement of the radioligand-receptor binding, the binding potential (BP) of [^{11}C]raclopride was calculated by the RPM with the

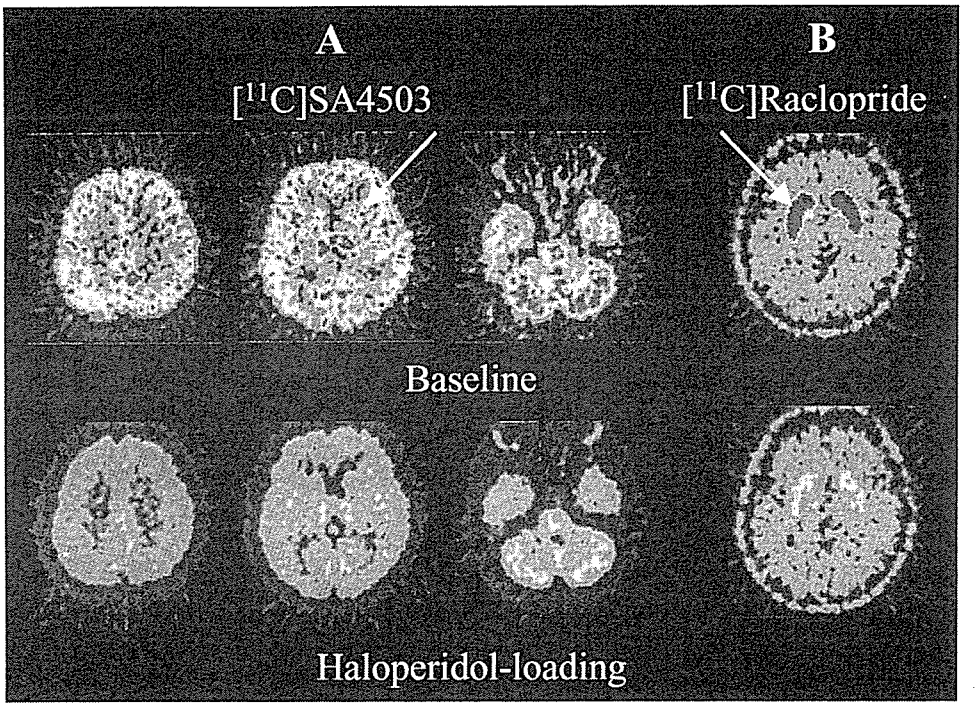

Fig. 1 PET images of [^{11}C]SA4503 (A) and [^{11}C]raclopride (B) in the same healthy subject in the baseline (*upper images*) and haloperidol-loading (*lower images*) conditions. The images of [^{11}C]SA4503 and [^{11}C]raclopride were acquired for 60–90 min and 40–60 min, respectively. White arrows show the striatum.

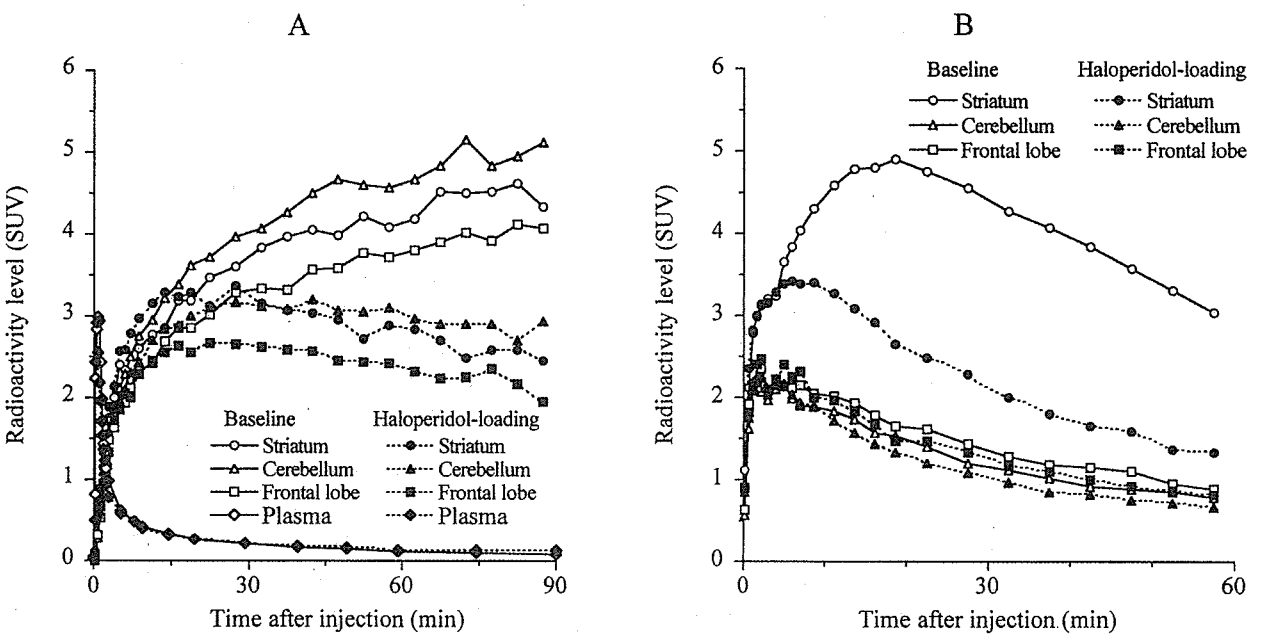

Fig. 2 Time-activity curves course of [^{11}C]SA4503 (A) and [^{11}C]raclopride (B) in the human brain and plasma in the baseline and haloperidol-loading conditions. Three regions of the brain were representatively selected: striatum (including caudate and putamen), cerebellum and frontal lobe.

cerebellum as a reference region.[15] For the binding of [^{11}C]SA4503, using the TACs of tissues and the metabolite-corrected TAC of plasma, the kinetic analysis was carried out based on a 2-tissue 3-compartment model having 4 parameters: K_1, influx rate constant from plasma to brain tissue; k_2, efflux rate constant from tissue to plasma; k_3, association rate constant between [^{11}C]SA4503 and sigma$_1$ receptor; and k_4, dissociation rate constant of

[^{11}C]SA4503-receptor complex.[9] The BP was expressed as k_3/k_4. The detailed validation of kinetic analysis of [^{11}C]SA4503 will be described elsewhere. The receptor occupancy (%) was defined as 100 × [(BP in baseline) – (BP in haloperidol-loading)]/(BP in baseline).

RESULTS AND DISCUSSION

Static PET images of [^{11}C]SA4503 and [^{11}C]raclopride in the baseline and haloperidol-loading conditions are represented in Figure 1. In the baseline, [^{11}C]SA4503 was taken up in all regions, whereas [^{11}C]raclopride was highly concentrated in the striatum. By the haloperidol-loading, the uptake of [^{11}C]SA4503 was reduced in all brain regions, while that of [^{11}C]raclopride was blocked in the striatum. The TACs in the striatum, cerebellum, frontal lobe and plasma are represented in Figure 2. The levels of radioactivity in plasma rapidly decreased to a similar extent in the two conditions. In the baseline measurement of [^{11}C]SA4503, the levels of radioactivity increased in all seven regions of the brain over 90 min in the case of Figure 2, or reached an apparent equilibrium state for 60 to 90 min in the other case (not shown), whereas the levels reached a plateau for 15–30 min and then decreased in the haloperidol-loading. The mean SUV values of [^{11}C]SA4503 for 60–90 min in the haloperidol-loading ranged approximately 55–65% of those in the baseline in the seven regions. BP was greatly reduced and the σ1R occupancy rates by haloperidol were approximately 80% in the seven regions investigated (Table 1).

In the case of [^{11}C]raclopride, the striatal uptake was greatly reduced by haloperidol-loading, while the levels of radioactivity in the other regions were not influenced by the haloperidol-treatment. The D2R occupancy rates based on BP values were 64% and 62% in the caudate and putamen, respectively (Table 1).

A number of neuroleptics possess moderate to high affinity for sigma binding sites, suggesting the possibility that sigma receptors mediate some of the antipsychotic effects of neuroleptics.[4] Frieboes et al. reported that haloperidol and the specific sigma ligand panamesine have similar antipsychotic properties regarding immunomodulation and sleep-electroencephalographic changes.[16] These findings suggest indirectly the binding of haloperidol to sigma receptors. The present study directly demonstrated the binding of haloperidol to σ1Rs in the human brain by [^{11}C]SA4503-PET. It is notable that the σ1R occupancy rates by haloperidol were larger than the D2R occupancy rates. A similar finding was previously observed in mice using a tissue dissection technique.[11] However, the present and previous studies indicated no association between σ1R occupancy rates and antipsychotic efficacy of haloperidol. Thus, evaluation of the σ1R occupancy rates by haloperidol or other antipsychotic drugs in relation to behavioral potency in humans by [^{11}C]SA4503-PET is of great interest.

In the present study, we performed quantitative evaluation of the binding of [^{11}C]SA4503 to σ1Rs using a standard method based on a 2-tissue 3-compartment model having 4 parameters. We also applied the graphical analysis using a Logan plot to the quantitative evaluation.[17] The Logan plot is a suitable method for parametric imaging of ligand-receptor binding because of its algorithmic simplicity and fast calculation speed, but it provides total distribution volume including both specific and non-specific binding, but not BP. However, the results showed good agreement in the receptor occupancy rates between BP and DVt, and it implied that the receptor density of σ1Rs could be visualized using Logan plot. The details will be described elsewhere.

In conclusion, [^{11}C]SA4503-PET can be used for evaluating σ1R occupancy rates by neuroleptics or other drugs. The technique could be valuable for developing new drugs and for evaluating the therapeutic effects of drugs in term of σ1R occupancy.

ACKNOWLEDGMENTS

This work was supported by Grants-in-Aid for Scientific Research (B) No. 13557077 and Scientific Research (C) No. 18591373 and for JSPS Fellows No. 18-6916 from the Japan Society for the Promotion of Science. The authors thank Ms. Miyoko Ando for her care of the subjects undergoing PET measurement.

REFERENCES

1. Kasper S, Tauscher J, Kufferle B, Barnas C, Pezawas L, Quiner S. Dopamine- and serotonin-receptors in schizophrenia: results of imaging-studies and implications for pharmacotherapy in schizophrenia. *Eur Arch Psychiatry Clin Neurosci* 1999; 249 (Suppl 4): 83–89.
2. Nyberg S, Nilsson U, Okubo Y, Halldin C, Farde L. Implications of brain imaging for the management of schizophrenia. *Int Clin Psychopharmacol* 1998; 13 (Suppl 3): S15–S20.
3. Tashiro M, Mochizuki H, Sakurada Y, Ishii K, Oda K, Kimura Y, et al. Brain histamine H_1 receptor occupancy of orally administered antihistamines measured by positron emission tomography with ^{11}C-doxepin in a placebo-controlled crossover study design in healthy volunteers: a comparison of olopatadine and ketotifen. *Br J Clin Pharmacol* 2006; 61: 16–26.
4. Debonnel G, de Montigny C. Modulation of NMDA and dopaminergic neurotransmissions by sigma ligands: possible implications for the treatment of psychiatric disorders. *Life Sci* 1996; 58: 721–734.
5. Walker JM, Bowen WD, Walker FO, Matsumoto RR, de Costa B, Rice KC. Sigma receptors: biology and function. *Pharmacol Rev* 1990; 42: 355–402.
6. Hashimoto K, Ishiwata K. Sigma receptor ligands: Possible application as therapeutic drugs and as radiopharmaceuticals. *Curr Pharm Design* 2006; 12: 3915–3928.
7. Kawamura K, Ishiwata K, Tajima H, Ishii S, Matsuno K, Homma Y, et al. *In vivo* evaluation of [^{11}C]SA4503 as a PET

ligand for mapping CNS sigma$_1$ receptors. *Nucl Med Biol* 2000; 27: 255–261.
8. Kawamura K, Ishiwata K, Shimada Y, Kimura Y, Kobayashi T, Matsuno K, et al. Preclinical evaluation of [^{11}C]SA4503: radiation dosimetry, *in vivo* selectivity and PET imaging of sigma$_1$ receptors in the cat brain. *Ann Nucl Med* 2000; 14: 285–292.
9. Kawamura K, Kimura Y, Tsukada H, Kobayashi T, Nishiyama S, Kakiuchi T, et al. An increase of sigma$_1$ receptors in the aged monkey brain. *Neurobiol Aging* 2003; 24: 745–752.
10. Mishina M, Ishiwata K, Ishii K, Kitamura S, Kimura Y, Kawamura K, et al. Function of sigma$_1$ receptors in Parkinson's disease. *Acta Neurologica* 2005; 112: 103–107.
11. Ishiwata K, Kawamura K, Kobayashi T, Matsuno K. Sigma$_1$ and dopamine D_2 receptors occupancy in the mouse brain after a single administration of haloperidol and two dopamine D_2-like receptor ligands. *Nucl Med Biol* 2003: 30: 429–434.
12. Fujiwara T, Watanuki S, Yamamoto S, Miyake M, Seo S, Itoh M, et al. Performance evaluation of a large axial field-of-view PET scanner: SET-2400W. *Ann Nucl Med* 1997; 11: 307–313.
13. Langer O, Någren K, Dolle F, Lundkvist C, Sandell J, Swahn CG, et al. Precursor synthesis and radiolabelling of the dopamine D_2 receptor ligand [^{11}C]raclopride from [^{11}C]methyl triflate. *J Label Compds Radiopharm* 1999; 42: 1183–1193.
14. Defrise M, Kinahan PE, Townsend DW, Michel C, Sibomana M, Newport DF. Exact and approximate rebinning algorithms for 3-D PET data. *IEEE Trans Med Imaging* 1997; 16: 145–158.
15. Gunn RN, Lammertsma AA, Hume SP, Cunningham VJ. Parametric imaging of ligand-receptor binding in PET using a simplified reference region model. *NeuroImage* 1997; 6: 279–287.
16. Frieboes RM, Murck H, Antonijevic I, Kraus T, Hinze-Selch D, Pollmacher T, et al. Characterization of the sigma ligand panamesine, a potential antipsychotic, by immune response in patients with schizophrenia and by sleep-EEG changes in normal controls. *Psychopharmacology (Berl)* 1999; 141: 107–110.
17. Logan J, Fowler JS, Volkow ND, Wolf AP, Dewey SL, Schlyer DJ, et al. Graphical analysis of reversible radioligand binding from time-activity measurements applied to [*N*-^{11}C-methyl]-(–)-cocaine PET studies in human subjects. *J Cereb Blood Flow Meta* 1990; 10: 740–747.

doi:10.1093/brain/awh713 *Brain* (2006), **129**, 791–808

Multimodal imaging of brain reorganization in motor areas of the contralesional hemisphere of well recovered patients after capsular stroke

Christian Gerloff,[1,2] Khalaf Bushara,[2] Alexandra Sailer,[1] Eric M. Wassermann,[4] Robert Chen,[2] Takahiro Matsuoka,[2] Daniel Waldvogel,[2] George F. Wittenberg,[3] Kenji Ishii,[2] Leonardo G. Cohen[3] and Mark Hallett[2]

[1]Cortical Physiology Research Group, Department of Neurology, Eberhard–Karls University Medical School, Tuebingen, Germany; Sections of [2]Human Motor Control and [3] Human Cortical Physiology, Medical Neurology Branch and [4] Brain Stimulation Unit, National Institute of Neurological Disorders and Stroke, National Institutes of Health, Bethesda, MD, USA

Correspondence to: Christian Gerloff, MD, Department of General Neurology, Hertie Institute for Clinical Brain Research, University of Tuebingen, Hoppe-Seyler Street 3, 72076 Tuebingen, Germany E-mail: christian.gerloff@uni-tuebingen.de or Mark Hallett, MD, NINDS, National Institutes of Health, 10 Center Drive, MSC-1428, Bethesda, Maryland 20892, USA, E-mail: hallettm@ninds.nih.gov

Clinical recovery after stroke can be significant and has been attributed to plastic reorganization and recruitment of novel areas previously not engaged in a given task. As equivocal results have been reported in studies using single imaging or electrophysiological methods, here we applied an integrative multimodal approach to a group of well-recovered chronic stroke patients (n = 11; aged 50–81 years) with left capsular lesions. Focal activation during recovered hand movements was assessed with EEG spectral analysis and $H_2{}^{15}O$-PET with EMG monitoring, cortico–cortical connectivity with EEG coherence analysis (cortico–cortical coherence) and corticospinal connectivity with transcranial magnetic stimulation (TMS). As seen from comparisons with age-matched controls, our patients showed enhanced recruitment of the lateral premotor cortex of the lesioned hemisphere [Brodmann area (BA) 6], lateral premotor and to a lesser extent primary sensorimotor and parietal cortex of the contralesional hemisphere (CON-H; BA 4 and superior parietal lobule) and left cerebellum (patients versus controls, $Z > 3.09$). EEG coherence analysis showed that after stroke cortico–cortical connections were reduced in the stroke hemisphere but relatively increased in the CON-H (ANOVA, contrast analysis, $P < 0.05$), suggesting a shift of functional connectivity towards the CON-H. Nevertheless, fast conducting corticospinal transmission originated exclusively from the lesioned hemisphere. No direct ipsilateral motor evoked potentials (MEPs) could be elicited with TMS over the contralesional primary motor cortex (iM1) in stroke patients. We conclude that (i) effective recovery is based on enhanced utilization of ipsi- and contralesional resources, (ii) basic corticospinal commands arise from the lesioned hemisphere without recruitment of ('latent') uncrossed corticospinal tract fibres and (iii) increased contralesional activity probably facilitates control of recovered motor function by operating at a higher-order processing level, similar to but not identical with the extended network concerned with complex movements in healthy subjects.

Keywords: Plasticity; stroke; recovery; motor control; motor cortex

Abbreviations: APB = abductor pollicis brevis muscle; BA = Brodmann area; COG = center of gravity; CON-H = contralesional hemisphere; DAM-H = damaged (stroke) hemisphere; EOI = electrode of interest; EDC = extensor digitorum communis; ERD = event-related desynchronization; FWHM = full width at half maximum; iM1 = ipsilateral (= contralesional) primary motor cortex; M1 = primary motor cortex; MEP = motor evoked potential; MRC = Medical Research Council; MT = motor threshold; NAP = number of active positions (from which TMS responses are elicited); OP = optimal point for eliciting a defined muscle response with TMS; POI = (electrode) pairs of interest; PT = pyramidal tract; rCBF = regional cerebral blood flow; ROI = region of interest; SMA = supplementary motor area; SPL = superior parietal lobule; SPM = statistical parametric map; tDCS = transcranial direct current stimulation; $\tanh^{-1}$ = inverse hyperbolic tangent; TMS = transcranial magnetic stimulation; TRCoh = task-related coherence; TrlogPow = task-related log-transformed power; TRPow = task-related power; TRtanh^{-1}Coh = task-related inverse hyperbolic tangent-transformed coherence

Received July 31, 2005. Revised September 29, 2005. Accepted November 7, 2005. Advance Access publication December 19, 2005

Introduction

Clinical recovery after stroke can be significant and has been attributed to plastic reorganization in the adult human CNS (Chollet *et al.*, 1991; Weiller *et al.*, 1992; Hamdy and Rothwell, 1998; Xerri *et al.*, 1998; Calautti and Baron, 2003; Cramer, 2003; Nudo, 2003; Ward *et al.*, 2003; Rossini and Dal Forno, 2004). Reorganization commonly refers to recruitment of areas previously not (or less) engaged in a given task, in order to substitute for directly lesioned or disconnected areas (Merzenich and Jenkins, 1993; Nudo *et al.*, 1996; Cramer *et al.*, 2001; Ward *et al.*, 2003; Baron *et al.*, 2004; Rossini and Dal Forno, 2004). A clinically relevant model for recovery is capsular stroke, with loss of corticospinal control from the primary motor cortex (M1) after a subcortical lesion of the efferent pyramidal tract (PT) fibers. In addition to areas located in the hemisphere of the ischaemic lesion (damaged hemisphere, DAM-H), homologous areas of the intact (contralesional) hemisphere (CON-H) have been considered candidates for taking over motor function after hemiparetic stroke (Chollet *et al.*, 1991; Feydy *et al.*, 2002; Fujii and Nakada, 2003) or language processing in patients with aphasia (Weiller *et al.*, 1995; Karbe *et al.*, 1998; Winhuisen *et al.*, 2005). It has been demonstrated that an extended premotor and sensorimotor network including those areas shows high metabolic activity during early clinical improvement with a linear decrease of activation towards later stages of recovery (Ward *et al.*, 2003; Fridman *et al.*, 2004). For capsular infarction with contralateral hemiparesis, a relevant candidate region is the M1 of the CON-H, ipsilateral to the paralysed limb (also referred to as 'ipsilateral M1', iM1). The present study specifically addresses the hypothesis that iM1 contributes to recovered motor function of the paretic hand in subcortical stroke.

It has been suggested that pre-existing uncrossed motor pathways originating from the iM1 may be accessed or recruited to compensate for damage to the crossed pathways after ischaemic stroke (Fisher, 1992; Cao *et al.*, 1998; Ago *et al.*, 2003). However, the data concerning the contribution of iM1 and other cortical regions of the CON-H are inconsistent. Evidence for involvement of iM1 in successful reorganization after stroke has been found in some studies (Chollet *et al.*, 1991; Cao *et al.*, 1998; Green *et al.*, 1999; Feydy *et al.*, 2002; Fujii and Nakada, 2003; Ward *et al.*, 2003) but not in others (Weiller *et al.*, 1992), and, in some, only if movements of the recovered limb were accompanied by mirror movements in the healthy limb (Weiller *et al.*, 1993). The latter finding points to a critical uncertainty in imaging studies on iM1 function after stroke, that is, the lack of sufficient control for mirror activity in the healthy limb when the paralysed limb is moved (Wittenberg *et al.*, 2000). The situation is complicated further because several investigations have pooled data from various types of lesions, for example, cortical and subcortical, supra- and infra-tentorial, left and right hemisphere of right- and left-handed patients with varied clinical outcomes (Cramer *et al.*, 1997; Ward *et al.*, 2003). Some findings with transcranial magnetic stimulation (TMS) have even suggested that enhanced ipsilateral responses to TMS over the iM1 are associated with poor clinical outcome (Netz *et al.*, 1997; Turton *et al.*, 1996). These data raised the possibility that iM1 activation could be interfering with recovery rather than helping it in some patients with predominantly subcortical lesions and moderate to good recovery (Martin *et al.*, 2004; Murase *et al.*, 2004; Ward and Cohen, 2004; Hummel *et al.*, 2005). More recently, studies have pointed to a functionally relevant contribution of the ipsilateral dorsal premotor cortex (iPMd) to recovered motor behaviour after stroke predominantly in patients with more prominent impairment rather than of the iM1 (Johansen-Berg *et al.*, 2002*a*).

To clarify some aspects of the contribution of iM1 and related motor structures (e.g. premotor cortex) of the CON-H to recovery after capsular stroke, we conducted a multimodal study combining clinical, anatomical, functional imaging and neurophysiological information in 11 patients with chronic ischaemic lesions of the left internal capsule. These methods provide complementary, rather than just mutually validating information, as they assess different aspects of information processing (PET, EEG) and functional connectivity (EEG, TMS). The identification of regions engaged in the recovery of function after focal CNS lesions is important not only from a basic science perspective but also from a clinical point of view. Approaches are evolving that might in the future allow for controlled focal enhancement of plastic adaptation in the cortex (e.g. repetitive TMS, convergent pair-pulse stimulation, epidural stimulation, transcranial direct current stimulation (tDCS)) (Stefan *et al.*, 2002; Brown *et al.*, 2003; Kobayashi *et al.*, 2003; Hummel and Gerloff, 2005) or for feeding cortical signals into prosthetic devices (Wessberg *et al.*, 2000; Wolpaw *et al.*, 2002; Friehs *et al.*, 2004; Kennedy *et al.*, 2004). To apply these techniques effectively, the target regions and their potential contributions must be known.

Patients and methods

All participants gave their written informed consent to each experiment according to the declaration of Helsinki (http://www.wma.net/e/ethicsunit/helsinki.htm), and the National Institute of Neurological Disorders and Stroke Institutional Review Board approved the study protocol. Patients were recruited by advertising in newspapers, to local doctors and by talking at local stroke clubs.

Patient inclusion criteria and clinical data

Inclusion criteria were (i) clinical diagnosis of a first-ever ischaemic stroke in the chronic stage (>8 months after the event; 'first-ever' stroke was clinically defined, small lacunar lesions without clinical consequences were not excluded), (ii) right-handedness according to the Edinburgh handedness inventory and (iii) subcortical lesion affecting the posterior limb of the left internal capsule. The lesions were documented by magnetic resonance imaging

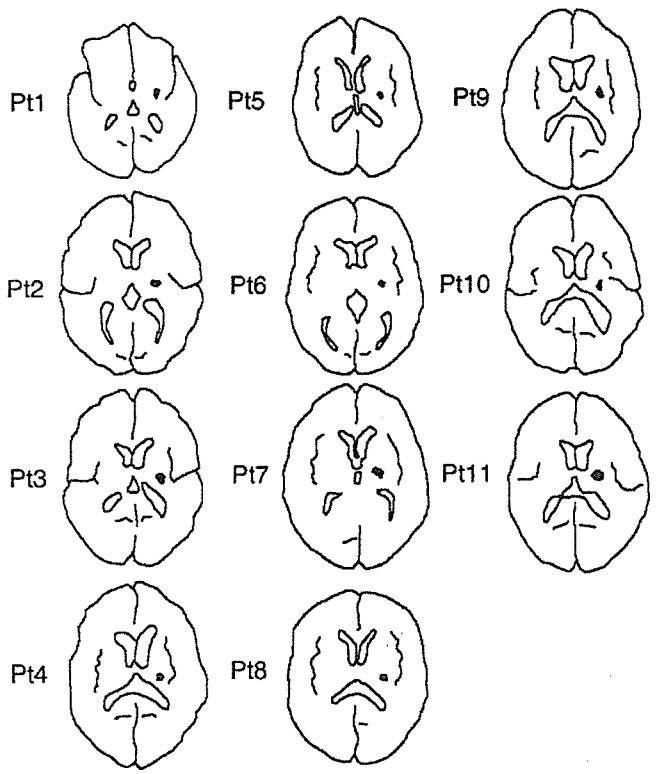

Fig. 1 Schematic representation of MRI lesion sites. Patient numbers correspond with those in the Table 1.

(MRI, T_1- and T_2-weighted images; 1.5 T GE scanner) (schematic drawings of the lesions are given in Fig. 1). Additional lacunar lesions were accepted only if there had not been any previous clinical stroke-like event, and if they were not located in the course of the PT of either hemisphere. The inclusion criterion for muscular strength at the time of the study was '>3/5' assessed clinically using the Medical Research Council (MRC) scale. Further, clinical motor recovery of '>1/5' on the MRC scale and regaining the capacity of individual finger movements were required. Excluded were patients with neurological diseases other than stroke or with neuropsychiatric or neuropsychological deficits which could potentially compromise informed consent or compliance during the experiments. Exclusion criteria were also history of seizures (because of TMS) and professional use of musical instruments prior to the stroke.

Time since stroke was 2.5 years (median, range 1–9 years). The median age in the patient group (n = 11, 2 females) was 70 years (50–81), in the EEG control group (n = 11, 2 females) 59 (48–79), in the PET control group (n = 11, 2 females) 63 (27–75). All controls were also right handed. The initial motor deficit of the patients is documented in Table 1. All patients had experienced substantial clinical recovery. For the stroke patients' right hand the mean ± SD MRC score was 4.1 ± 0.4, for elbow flexion/extension 4.3 ± 0.5, for shoulder movements 4.3 ± 0.5 and for the right leg 4.0 ± 0.0. The left side was not affected in any of the patients. As for skilled movements, all patients needed to be able to perform a finger opposition task (index-to-thumb, middle finger-to-thumb, etc.), finger tapping and finger extensions at a rate of 1–2 per second without mirror activity in the concomitantly recorded EMG. All patients made use of their recovered hand in daily life activities (like holding a cup, tying shoe laces, buttoning a shirt). Grip force in patients was also quantified by a dynanometer. For the stroke patients' right hand the mean ± SD was 59 ± 32 lbs, for their healthy (left) hand the corresponding value was 84 ± 27 lbs. Deep tendon reflexes were increased on the right-hand side in 9 out of 11 patients, a slight somatosensory deficit (hypesthesia) was reported in 2 out of 11 patients.

EEG

EEG was recorded during two conditions: (i) metronome-paced extensions of fingers II–V at a rate of 1 per second with the right hand (MOVE) and (ii) listening to the metronome beats at 1 per second without moving (REST). Subjects were seated comfortably in an armchair with the right arm relaxed and resting on a pillow. The right hand was positioned palm down at the edge of the pillow so that the fingers could be moved freely. Subjects performed repetitive, brisk simultaneous finger extensions followed by brief relaxation (rather than voluntary flexion) (Fig. 2). To avoid intra-session learning effects, subjects practised the required movement before the EEG recording, using online EMG feedback. Five to ten blocks of 100 movements (corresponding to 100 s) and REST (also 100 s) were recorded, alternating with breaks of 1–5 min between blocks to avoid muscular fatigue. During all conditions, subjects looked at a stationary fixation point to prevent eye movements, and were instructed to avoid eye blinks, swallowing or any movement other than the required finger movements. Continuous EEG was recorded from 28 surface electrodes, mounted in a cap (Electro-Cap International Inc., Eaton, OH). Impedances were kept below 8 kΩ. Data were sampled at 250 Hz, low-pass filter was set at 50 Hz and the time constant was set to DC (DC amplifiers and software by Neuroscan, Inc., El Paso, TX). Linked earlobe electrodes served as reference. Four bipolar EMG channels were recorded from surface electrodes positioned over the right and left forearm extensors (extensor digitorum communis, extensor carpi radialis), with each pair of electrodes located ~15 cm apart (distal tendon reference). The high-pass filter for EMG was set to 30 Hz.

The EEG data were analysed using two different approaches: (i) task-related power (TRPow) and event-related desynchronization (ERD) to assess regional activation and its time course and (ii) task-related coherence (TRCoh) to assess interregional coupling.

For analysis of TRPow, EEG signals were digitally filtered off-line (1–50 Hz, slope 24 dB/octave) and, for each experimental condition separately, segmented into non-overlapping epochs (= disjoint sections; cf. Amjad *et al.*, 1997) of 1024 ms (allowing a frequency resolution of 1 Hz). After removal of slow drifts by linear trend correction and baseline correction (using the entire window from 0 to 1024 ms), the single sweeps were visually inspected, and trials with artifacts were rejected. On average, in the patient group 431 artifact-free trials (median) were obtained for the rest condition, 415 trials for the movement condition. In the control group, 458 artifact-free trials were obtained during rest, 447 during movement. Each single sweep was Hamming windowed to minimize spectral leakage. For spectral power analysis, a discrete Fourier transform was computed for each 1024 ms epoch and all electrodes. Spectral power (Pow) was calculated for 4 standard frequency bands: low alpha (8–10 Hz), high alpha (11–13 Hz), low beta (16–20 Hz) and high beta (22–26 Hz). In order to reduce the effect of inter-subject and inter-electrode variability of absolute spectral power values, task-related relative power at an electrode x ($TRPow_x$) was obtained by computing a ratio of rest ($Pow_{x\ rest}$) and corresponding activation conditions ($Pow_{x\ activation}$), according to the following

Table 1 Clinical data

Patient	Age (years)	Gender	Initial symptoms	Years after stroke	Residual symptoms	Localization of ischaemic lesions*						
						Left hemisphere						Right hemisphere
						ICP	GP	PUT	TH	CR	WML	
1	76	M	Right-hand side weakness, unable to walk, dysarthria	2.3	Slight right-hand clumsiness (MRC = 4), spasticity of leg, facial weakness	x	x	x			x	
2	73	F	Severe right hemiparesis, no other symptoms	7.0	Right-hand clumsiness, no weakness (MRC = 5)	x				x	x	
3	59	M	Right-arm paralysis, severe leg; hemiparesis, dysarthria	2.0	Moderate right-hand clumsiness; (MRC = 4), moderate spasticity	x	x	x		x	x	
4	60	M	Right-hand side weakness, unable to walk, dysarthria	2.5	Slight right-hand clumsiness (MRC = 4) Mild spasticity, facial weakness	x	x					PUT
5	73	F	Right-hand side hemiplegia, right visual field defect	7.2	Slight right arm paresis (MRC = 4) moderate spasticity	x	x	x		x	x	
6	61	M	Right-hand side hemiparesis (severe)	2.0	Mild spasticity right arm and hand (MRC = 4)	x						PUT
7	81	M	Right-hand side hemiparesis	4.1	Moderate right-hand weakness (MRC = 4-)	x						
8	50	M	Right-hand side hemiplegia, dysarthria	0.9	Moderate right-hand clumsiness, No weakness (MRC = 5)	x	x		x		x	
9	70	M	Right-hand side hemiparesis, dysarthria	3.6	Moderate right-hand clumsiness, limited use of right hand (MRC = 4-)	x	x	x			x	TH, ICP
10	75	M	Right-hand side hemiplegia, inability to speak	2.3	Moderate right-hand clumsiness, slight right-hand weakness (MRC = 4)	x		x	x		x	TH, ICP
11	66	M	Right-hand side hemiparesis, milder weakness of lower extremity	9.0	Slight right-hand clumsiness and weakness (MRC = 4)	x	x	x	x			PUT

*Lesions other than in the posterior limb of the left internal capsule (ICP) were lacunar and asymptomatic according to clinical history and neurological examination.
GP = globus pallidus; PUT = putamen; TH = thalamus; CR = corona radiata; WML =white matter lesions.

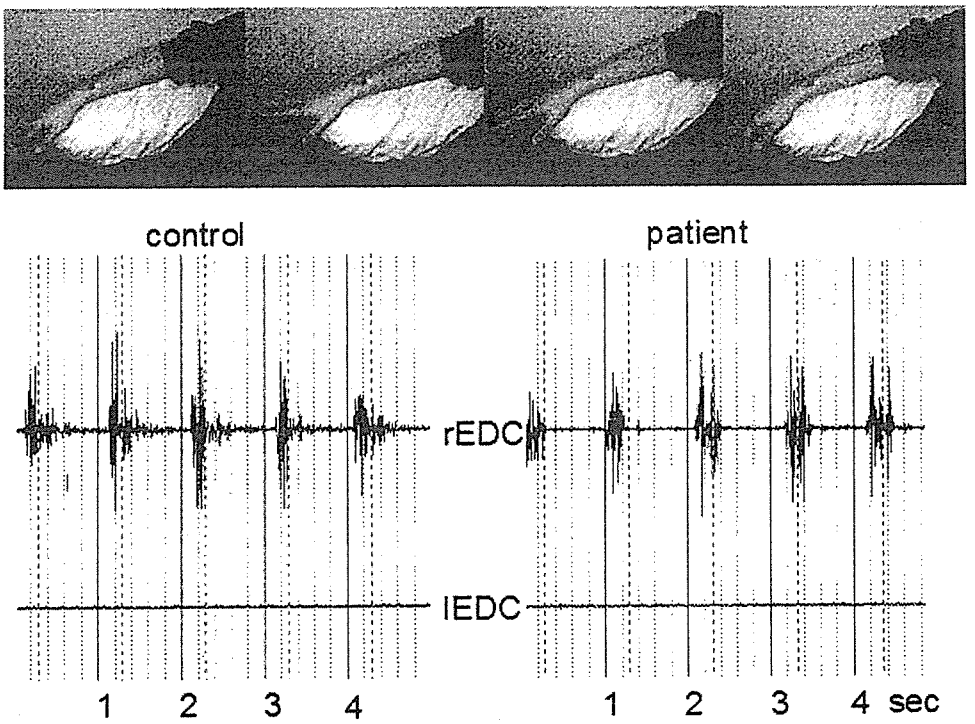

Fig. 2 Experimental paradigm. Top = the motor task consisted in brisk finger extensions at a rate of 1 per second. Bottom = EMG of bilateral forearm extensors (left and right extensor digitorum communis muscles, lEDC and rEDC) was monitored throughout all imaging procedures. Two representative traces are shown. Left = control subject, right = stroke patient. Absence of mirror activity in the hand at rest was required for all trials that entered the final analysis (PET, EEG).

equation.

$$\frac{\mathrm{Pow}_{x\ \mathrm{rest}} - \mathrm{Pow}_{x\ \mathrm{activation}}}{\mathrm{Pow}_{x\ \mathrm{rest}}} \times 100. \quad (1)$$

This approach and its statistical evaluation (including logarithmic, *log*, transformation to stabilize the variance) has been described elsewhere in detail (Pfurtscheller and Aranibar, 1977; Sailer *et al.*, 2000). Relative TRPow decreases ('activation') are expressed in per cent and as positive values. In topographic maps, 'activation' is coded by red colour. To assess the temporal evolution of spectral power changes, the technique of ERD was employed as described elsewhere in detail (Pfurtscheller and Andrew, 1999; Pfurtscheller *et al.*, 2003). This analysis was added in order to get supplementary information on the nature of the contralesional activation in the central region. If the nature of this activation would be linked to reafferent feedback or reflex-like activation of the contralesional motor system as has been proposed previously (Verleger *et al.*, 2003), it should occur only after movement onset; if it is related to movement preparation and execution, it needs to be present before and during movement. For ERD calculation, the raw EEG signal is band-pass filtered for the frequency range of interest (here, 16–20 Hz), rectified and averaged after epoching. The time course of spectral power changes is then plotted in relation to a baseline value (here, mean power during rest) as a function of time. As this type of baseline correction is used and spectral power during baseline (= rest) is typically higher than during activation (= movement), ERD ('activation') is represented as negative values. For the sake of comparability, topographic ERD maps were plotted like the maps for TRPow, i.e. 'activation' is coded in red.

Coherence is computed in the frequency domain and is a normalized measure of the coupling between two signals at any given frequency (Shaw, 1984; Classen *et al.*, 1998). For TRCoh analysis, EEG signals were filtered, segmented, trend and baseline corrected, inspected for artefacts, Hamming windowed and Fourier transformed as described for TRPow. The coherence values (Coh) were calculated for each frequency bin λ according to the following equation (commercial software by Neuroscan, Inc., El Paso, TX, USA).

$$\mathrm{Coh}_{xy}(\lambda) = |R_{xy}(\lambda)|^2 = \frac{|f_{xy}(\lambda)|^2}{f_{xx}(\lambda) f_{yy}(\lambda)} \quad (2)$$

The mathematical details as well as the statistical procedures for significance testing (including inverse hyperbolic tangent transformation, $\tanh^{-1}$, to stabilize the variance) have been reported elsewhere (Classen *et al.*, 1998; Andres *et al.*, 1999; Hummel and Gerloff, 2005). In order to reduce the effect of inter-subject and inter-electrode-pair variability of absolute coh, task-related relative coherence (TRCoh_{xy}) was obtained by subtracting rest ($\mathrm{Coh}_{xy\ \mathrm{rest}}$) from corresponding activation conditions ($\mathrm{Coh}_{xy\ \mathrm{activation}}$). Coherence magnitude increments ('coupling') are expressed as positive values, and coherence decrements are expressed as negative values. Coherence increments or decrements between baseline and movement conditions for each pair of electrodes were displayed as color-coded 'link' plots, which permit the inspection of the magnitude and spatial patterns of TRCoh. The subtractive approach also minimizes the bias in the absolute coherence introduced by volume conduction or the reference electrodes (Classen *et al.*, 1998; Fein *et al.*, 1988; Rappelsberger and Petsche, 1988). Broadband coherence was calculated for the same frequency bands as TRPow.

For statistical analysis, factorial ANOVA designs with contrast analyses were used on log-transformed TRPow or $\tanh^{-1}$ transformed TRCoh data (Gerloff *et al.*, 1998, 2003). For TRlogPow,

factors were group (patients, control) and region. For TRtanh^{-1}Coh, factors were group (patients, control) and connection. We have described the definition of regions and connections in a similar study on normal subjects in previous papers in detail (Gerloff *et al.*, 1998; Andres *et al.*, 1999). For TRPow analysis, nine electrodes of interest (EOI) were grouped into three regions each represented by three electrodes: 'left central' (FC3, C3, CP3), 'right central' (FC4, C4, CP4) and 'mesial frontocentral' (Fz, FCz, Cz). For TRCoh analysis, the total number of links between the EOIs was 27 (27 pairs of interest, POI), which were grouped into three major connections: 'left central to right central' (FC3–FC4, FC3–C4, FC3–CP4, C3–FC4, C3–C4, C3–CP4, CP3–FC4, CP3–C4, CP3–CP4), 'left central to mesial frontocentral' (FC3–Fz, FC3–FCz, FC3–Cz, C3–Fz, C3–FCz, C3–Cz, CP3–Fz, CP3–FCz, CP3–Cz) and 'right central to mesial frontocentral' (FC4–Fz, FC4–FCz, FC4–Cz, C4–Fz, C4–FCz, C4–Cz, CP4–Fz, CP4–FCz, CP4–Cz). Significance levels obtained from multiple tests on the same data pool were Bonferroni-corrected. Results were considered significant if $P < 0.05$ after correction.

$H_2{}^{15}O$ PET

PET scanning was performed during the same conditions as EEG, (i) metronome-paced extensions of fingers II–V at a rate of 1 per second with the right hand (MOVE) and (ii) listening to the metronome beats at 1 per second without moving (REST). Scans were obtained in 3D mode using a GE Advance PET tomograph (Waukesha, WI, USA) with an axial field of view of 15.3 cm, covering the whole brain. Task performance began 30 s before bolus infusion of 10 mCi of $H_2{}^{15}O$ (half life, 2.1 min) via a left cubital vein catheter. Scanning was started when a rising brain radioactivity count was first detected (20–30 s after radioisotope injection) and continued for 60 s thereafter. Arterial blood was not sampled and the radioactive counts were therefore used as a measure of relative rCBF (Herscovitch *et al.*, 1983). Five scans were obtained for each REST and MOVE conditions. Interscan interval was 10 min. A transmission scan was obtained prior to each session and used to correct for radioactivity attenuation. Head movement was minimized by using a thermoplastic mask molded to each subject's head and attached to the scanner bed. Attenuation-corrected scans were reconstructed into 35 transaxial planes, 4.25 mm apart, with an in-plane center resolution of 6.5 mm full width at half maximum (FWHM) in each direction. SPM99 software (http://www.fil.ion.ucl.ac.uk/spm) was used for realignment, normalization to a standard stereotactic space (Montreal Neurological Institute brain template) and smoothing with an isotropic Gaussian filter of 12 mm to accommodate individual variability in gyral anatomy.

After correcting for variations in global blood flow (normalized to 50 ml/100 cm ^{3}/min) using ANCOVA (analysis of covariance), differences between experimental conditions (using the contrast MOVE minus REST) were statistically tested for each voxel (search volume was from $z = -50$ to $z = 80$) with SPM99. The resulting whole-brain statistical parametric maps (SPMs) based on the *t*-statistic (transformed to normalized *Z*-scores) had a final spatial resolution of $x = 10.4$, $y = 11.8$, $z = 13.4$ mm (FWHM). We used a two-step random-effects method to determine between-group differences (Friston *et al.*, 1999; Woods, 1996). We applied a statistical significance threshold of peak activity at $Z > 3.09$ and used $P < 0.05$ with small volume correction of for prespecified regions in known motor areas (Poline *et al.*, 1997).

During PET scanning, EMG was monitored from bilateral forearm extensors and flexors with a Dantec Counterpoint unit (*A/D* rate, 5 kHz, band-pass filter 5 Hz–1.5 kHz; DANTEC Counterpoint electromyograph, DANTEC Medical A/S, Skovlunde, Denmark). Two subjects had to be excluded from PET analysis because their motor performance in the scanner did not match the performance of the nine other patients (different movement rate, different type of movement; non-compliance with the instructions in supine position).

Transcranial magnetic stimulation

TMS was performed using a magnetic stimulator (Cadwell Laboratories, Inc., Kennewick, WA) equipped with a focal 2 × 70 mm 'figure-of-eight' coil, and an EMG unit (*A/D* rate, 5 kHz, band-pass filter 5 Hz–1.5 kHz; DANTEC Counterpoint electromyograph, DANTEC Medical A/S, Skovlunde, Denmark). Motor evoked potentials (MEPs) were recorded simultaneously from both forearms using surface EMG electrodes attached over the patients' finger extensor muscles (extensor digitorum communis, EDC), 5 cm apart, or, in two patients, abductor pollicis brevis (APB) muscles, with the active electrode placed on the muscle belly and the inactive electrode over the base of the metacarpophalangeal joint of the thumb. MEPs can be facilitated by voluntary pre-contraction of the target muscles. With this technique, ipsilateral responses can be elicited even in some healthy adults (Wassermann *et al.*, 1994; Ziemann *et al.*, 1999). Thus, for the main part of the TMS experiment we opted to stimulate with the target muscles at rest. Only moderate pre-contraction (~5–10% maximum) was then used in a second run in order to test with higher sensitivity for ipsilateral responses. Continuous acoustic feedback of EMG activity in both forearms was provided during the entire examination. Both hemispheres were searched for stimulation points eliciting contra- or ipsilateral MEPs, and the optimal points (OP; defined as the scalp position where a reproducible muscle response was elicited with the lowest stimulation intensity) as well as their resting motor thresholds (MT; defined as the minimum stimulation intensity that produced at least 5 MEPs exceeding 50 μV in 10 trials) were determined separately. After detection of the OP and determination of MT, the cortical representation of the target muscle was mapped. For quantitative evaluation, the number of active positions (NAP) was computed. 'Active' was defined using a strict (a) and less conservative (b) cutoff. The cutoff for (a) was >50% of the amplitude when stimulated over OP, for (b) >25% of this amplitude. Topographical location was assessed further by calculation of the center of gravity (COG) of each map, according to following equation, i.e. the sum of the vectors of site position weighted individually by MEP amplitudes divided by the sum of all MEP amplitudes (Liepert *et al.*, 1999; Ziemann *et al.*, 1999).

$$\frac{\sum(\text{MEP} \times \text{site})}{\sum \text{MEP}} \quad (3)$$

The COG *x*- and *y*-coordinates are given relative to the vertex (=Cz position of the international 10/20 system of electrode placement). Negative *x*-values correspond to left-hemispheric positions, negative *y*-coordinates denote positions anterior to the vertex.

The absence of ipsilateral responses from the healthy hemisphere was documented by stimulation with 200% MT or 100% stimulator output (whatever was reached first) at the OP for contralateral responses, and at positions 1 and 2 cm anteriorly, posteriorly, laterally and medially.

MT, NAP and the coordinates of the COG were compared between DAM-H and CON-H using the Wilcoxon matched pairs test. The significance level was set at $P < 0.05$.

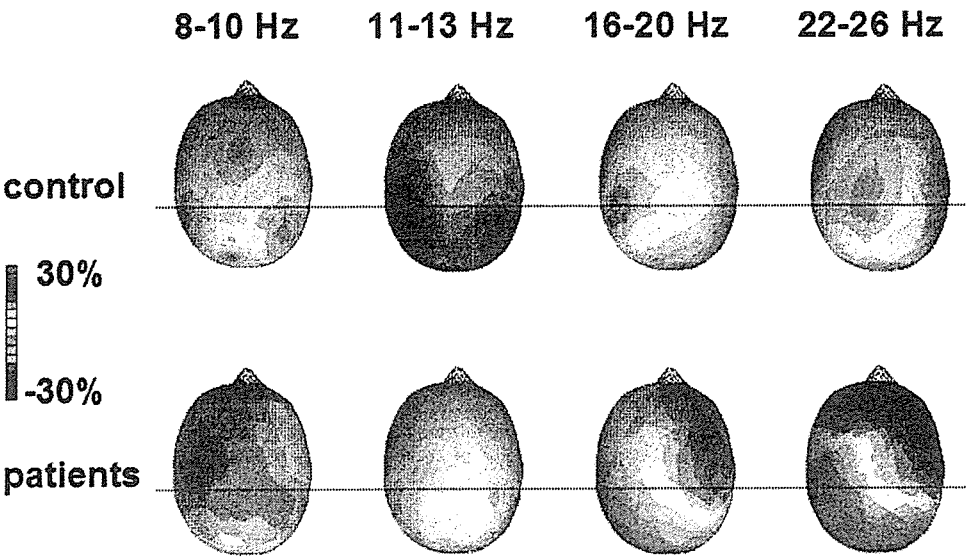

Fig. 3 Results of EEG spectral power analysis (TRPow). Grand average. Cortical activation (TRPow decreases, given in per cent with positive sign) is colour-coded in red. Top = control group, Bottom = stroke patients. The beta frequency band (16–20 and 22–26 Hz) is known to be particularly sensitive to variation of motor parameters in sensorimotor tasks. In this band, the main result was enhancement of activity in the CON-H of stroke patients, extending from the central region (dotted horizontal line) into the frontal and prefrontal cortex. In the alpha band, the results were more variable and only the global decrease of activation in the 11–13 Hz band was statistically significant. At 8–10 Hz, no significant differences were found. Right-hand side of each map = right-hand side of the brain.

Results

Spectral power and coherence analysis of the EEG

The amplitude of activation (TRPow) and the topographic pattern of activation were different for patients and controls (ANOVA, main effect group, $P = 0.0001$; interaction group x region, $P = 0.0001$). Figure 3 illustrates the topographic maps of cortical activation related to right-hand movements in both groups. Distinct patterns were found in normal controls in four frequency ranges (8–10 Hz, 11–13 Hz, 16–20 Hz, 22–26 Hz), in line with a previous EEG study on aged healthy subjects (Sailer *et al.*, 2000). The differences between patients and controls were significant in the high alpha band (11–13 Hz), and in the low and high beta band (16–20 Hz, 22–26 Hz). TRPow decreases (activation) in the (right) CON-H were larger in patients (ANOVA, contrast analysis, $P < 0.01$). In these frequency bands, TRPow decreases in the DAM-H (i.e. activation) were reduced in patients compared with the control group (ANOVA, contrast analysis, $P < 0.01$). In the low alpha band (8–10 Hz) there was a trend towards greater TRPow decreases in patients which, however, did not reach significance because of inter-subject variability.

The most pronounced enhancement of central region activity in the CON-H of patients occurred in the beta frequency range (16–20 Hz). Time-course analysis (16–20 Hz ERD) demonstrated that this enhanced activity in the right central region occurred both in the pre-movement phase and during movement execution (Fig. 4). Together with the known sensitivity of this frequency range to variation of motor parameters rather than somatosensory aspects of a task (Conway *et al.*, 1995; Pfurtscheller *et al.*, 1997; Mima *et al.*, 2000), the time-course data substantiate the notion that this contralesional overactivation is related to actual motor processing including preparation of the recovered movement.

The pattern of inter-regional functional coupling (TRCoh) between left and right central regions and between lateral central and frontomesial areas (including the region of the supplementary motor area, SMA) was also different in patients. TRCoh was generally lower after stroke (high alpha, low and high beta band; ANOVA, main effect group, $P < 0.0001$). In addition, TRCoh showed a relative, focal increase between right central and frontomesial cortex in patients (all frequencies; ANOVA, contrast analysis, $P < 0.05$), i.e. between the motor and premotor areas of the CON-H and the mesial premotor structures (like SMA). In addition to the marked convergence of coherence links to the right central region, the ipsilesional (left) central region (e.g. electrode C3, DAM-H) also showed links to mesial and contralateral premotor and sensorimotor areas (low beta band). The topographic coherence maps are displayed in Fig. 5.

Statistical parametric mapping of rCBF ($H_2{}^{15}O$-PET)

Movements were associated with activation of known sensorimotor structures such as left primary motor and primary somatosensory cortex (BA 4 and BA 3), left SMA (BA 6), left PMd (BA 6), left insula (BA 13), basal ganglia (claustrum, thalamus) and cerebellum. Details are given in Table 2.

On direct comparison with the control group, right-hand movements in patients were associated with increased activation of several areas in both the DAM-H (left) and CON-H